Available online at www.sciencedirect.com
ScienceDirect
International Journal of Solids and Structures 44 (2007) 8143–8158
INTERNATIONAL JOURNAL OF SOLIDS AND STRUCTURES
www.elsevier.com/locate/ijsolstr

Effect of permanent indentation on the delamination threshold for small mass impact on plates

D. Zheng, W.K. Binienda *

Department of Civil Engineering, The University of Akron, Akron, OH 44325-3905, USA

Received 17 January 2007; received in revised form 6 June 2007; accepted 7 June 2007
Available online 14 June 2007

Abstract

Small mass impacts on composite structures are common cases caused by hailstones and runway debris. Small mass impactors usually result in a wave controlled local response, which is independent of boundary conditions. This response occurs before the reflection of waves from the boundaries and cannot be modeled by large mass drop weight tests. An elasto-plastic contact law, which accounts for permanent indentation and damage effects, was used here to study small mass impact on laminated composite plates. By comparing with results from the Hertzian contact law, it was found that damage can change the dynamic response of the structure significantly with increasing impact velocity. Due to smaller contact force generated for the case of using elasto-plastic contact, the central displacement of the plate is also less than the one using Hertzian contact law. The linearized version of the contact law was then used to derive the closed-form approximations of the contact force, indentation and plate central displacement for the impact loading of composite laminates. The threshold velocity for delamination onset under small mass impact was predicted analytically based on the obtained peak contact forces by combining with an existing quasi-static delamination threshold load criterion. A good agreement was found between the predicted threshold values and published experimental results.

Keywords: Contact law; Impact damage; Analytical modeling; Delamination; Threshold; Laminated composites

1. Introduction

Fiber-reinforced composites are being utilized as viable alternatives to metallic materials in structures where weight is a major consideration, e.g., aerospace structures, high-speed boats and trains. However, a well-known problem with composite laminates is their poor resistance to accidental impact by foreign objects. The resulting damage due to impacts, often in the form of delaminations, matrix cracking and fiber failures may severely reduce the structural strength and stability (Abrate, 1991). Therefore, considerable amount of research has been done in the area of impact of composite structures.

Impacts are often termed as low-velocity and high-velocity impacts. However, a more relevant classification was proposed by Olsson (1992) as boundary-controlled and wave-controlled impact. For boundary-controlled

* Corresponding author. Tel.: +1 330 972 6693; fax: +1 330 972 6020.
E-mail address: wieslaw@uakron.edu (W.K. Binienda).

0020-7683/$ - see front matter © 2007 Elsevier Ltd. All rights reserved.
doi:10.1016/j.ijsolstr.2007.06.005

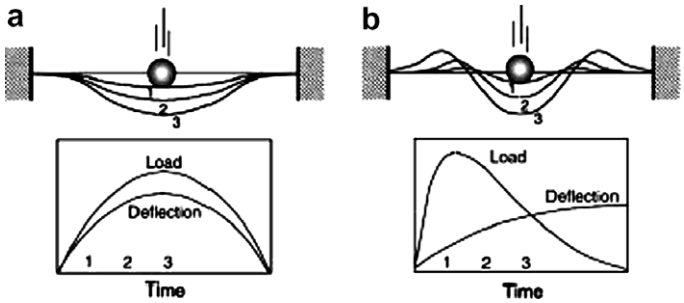

Fig. 1. Comparison between boundary-controlled and wave-controlled Impact (Olsson, 2003).

impact, the entire plate is deformed during the impact, and the contact force and plate deformation are more or less in phase, as shown in Fig. 1a. However, for wave-controlled impact, the plate deformation is localized to the region around the impact point, and the contact force and plate deformation are never in phase, as shown in Fig. 1b. Generally, boundary-controlled and wave-controlled impacts are associated with large-mass and small-mass impact responses. A mass-ratio based criterion governing boundary-controlled and wave-controlled impact response has been derived in detail by Olsson (2000). It was shown that small mass impact occurs when the mass of the impactor is less than one-fourth of the mass of the largest possible area for which waves do not interfere with the boundaries.

Due to the more localized deformation, small-mass impacts cause higher impact forces and earlier damage initiation than large-mass impacts with the same kinetic energy. Usually, the initial matrix cracking is attributed to high contact stresses that initiate at relatively low-loads. However, the onset of delamination typically happens at higher impact loads. Therefore, the peak contact force becomes a key parameter and determines the criticality of the impact during small mass impact (Christopherson et al., 2005). For boundary-controlled quasi-static impacts, the delamination threshold load has been derived and validated by experimental data (Olsson, 2001). The concept of mobility, which describes the velocity per unit force under sinusoidal excitation of linear systems, was used to predict the peak contact force as well as delamination threshold velocity for wave-controlled impact loading of composite laminates (Olsson, 2003; Olsson et al., 2006). Mobility is a frequency dependent quantity and the mobility of serial systems is obtained by adding the mobility of subsystems.

Most of the above impact models for wave-controlled and boundary-controlled impacts are based on Hertzian contact law. The Hertzian contact law was obtained from the elastostatic analysis of contact between the spherical impactor and elastic half-space where permanent deformations due to damage were not accounted for. During the initial stages of impact loading, Hertzian-type contact laws are adequate for most cases. However, it has been shown that even at low contact loads, the permanent deformation causing damages around the contact zone is present, and the unloading phase of the process is significantly different from the loading phase (Yang and Sun, 1982; Tan and Sun, 1985; Cairns, 1991). Chattopadhyay and Saxena (1991) investigated the combined effects of shear deformation and permanent indentation on the impact response of elastic isotropic plates based on a modified Hertzian contact law with recovery process. In this paper, an elasto-plastic contact law proposed by Yigit and Christoforou (1994), which accounts for permanent indentation and damage effects, was used to study small mass impact on laminated composite plates. Closed-form approximation of the peak contact force obtained from the linearized elasto-plastic contact law was then employed to predict the threshold velocity for delamination onset. The methodology presented in this study is valuable in designing model tests for small mass impacts on composite structures.

2. Derivation of the governing equations

The formulation of the governing equations is based on the original work done by Olsson (1992). A basic assumption in this formulation is that the time involved is so short that the bending waves do not reflect back from the boundaries of the plate, i.e., in the "early state" of the impact phenomenon. It has been analytically shown, as may be intuitively expected, that the boundary conditions have no influence on the dynamic

response of the structures during the "early state" (Mittal, 1987). In particular, if the impact lasts for a period much less than the time taken for the return of the fastest flexure waves to the point of impact, then the structure can be assumed infinite.

The analysis was based on Kirchhoff's plate theory for specially orthotropic composite plates with zero damping. It was shown that the plate center deflection at impact point $(0,0)$ can be written as

$$w_p(0,0,t) = \frac{1}{8\sqrt{m_p D^*}} \int_0^t F(\tau)\mathrm{d}\tau \tag{1}$$

where the effective plate stiffness D^* is defined by fairly complicated expressions including elliptical integrals but a sufficient approximation is (Olsson, 2003):

$$\begin{aligned} D^* &= \sqrt{D_{11}D_{22}(A+1)/2} \\ A &= (D_{12}+2D_{66})/\sqrt{D_{11}D_{22}} \end{aligned} \tag{2}$$

where D_{ij} are called the bending stiffnesses which can be calculated from laminate theory.

By neglecting the vibrations in the impactor, the displacement of the impactor and the initial conditions can be expressed as

$$\begin{aligned} w_i(t) &= V_0 t - \frac{1}{m_i}\int_0^t \int_0^\tau F(\xi)\mathrm{d}\xi\mathrm{d}\tau \\ w_i(0) &= 0, \quad \dot{w}_i(0) = V_0 \end{aligned} \tag{3}$$

The indentation of the plate is defined by

$$\alpha = w_i - w_p \tag{4}$$

Differentiating the above equation twice with respect to time, the indentation is governed by the differential equation

$$\begin{aligned} &\frac{\mathrm{d}^2\alpha}{\mathrm{d}t^2} + \frac{1}{8\sqrt{m_p D^*}}\frac{\mathrm{d}F}{\mathrm{d}t} + \frac{F}{m_i} = 0 \\ &\alpha(0) = 0, \quad \dot{\alpha}(0) = V_0 \end{aligned} \tag{5}$$

3. Contact laws

3.1. Hertzian contact law

In the original study done by Olsson (1992), Hertzian contact law was used to describe the contact phenomenon. According to Hertzian theory developed for static loading on isotropic linear elastic half-space, the relationship between contact load and the indentation can be described as (Goldsmith, 1960)

$$F(\alpha) = k_h \alpha^{3/2} \tag{6}$$

where k_h is the contact stiffness and

$$k_h = \tfrac{4}{3} Q_\alpha \sqrt{R} \tag{7}$$

with

$$1/Q_\alpha = 1/Q_{zi} + 1/Q_{zp} \tag{8a}$$

$$Q_{zk} = E_{zk}/(1 - v_{rzk}v_{zrk}), \qquad k = i,p \tag{8b}$$

where R is the impactor nose radius, and E_{zk} is the modulus in the thickness direction of body k, and v_{rzk} and v_{zrk} are the different Poisson's ratios for body k. When the impactor is much stiffer than the plate, Eq. (8a) simplifies to

$$1/Q_\alpha = 1/Q_{zp} \tag{9}$$

As shown recently by Swanson (2005), Hertzian contact law for impact on isotropic half-space can be extended to impact on transversely isotropic plate with finite thickness, if the isotropic modulus is replaced by a combination of transversely isotropic properties. Thus, for normal contact on transversely isotropic plate with finite thickness, the relationship between contact load and the indentation can be described as

$$F(\alpha) = \beta k_h \alpha^{3/2} \tag{10}$$

where k_h is the contact stiffness defined in Eq. (7) except that the effective modulus Q_{zp} is replaced for transversely isotropic materials.

In Eq. (10), β is an empirical constant accounting for contact force reduction in finite thickness plate relative to half-space contact loading of orthotropic materials. The effect of finite thickness of the plate on the indentation stiffness was studied numerically by Suemasu et al. (1994). It was shown that the contact stiffness is smaller in finite thickness plates than is predicted from contact loading on a half-space.

It was shown by Turner (1979) that the effective modulus for transversely isotropic normal contact can be expressed as

$$Q_{zp} = \frac{2}{\alpha_1 \alpha_3} \tag{11}$$

with

$$\alpha_1 = \sqrt{\frac{E_x/E_z - v_{xz}^2}{1 - v_{xy}^2}} \tag{12a}$$

$$\alpha_2 = \frac{1 + \left(\frac{E_x}{2G_{xz}} - 1\right) - v_{xz}(1 + v_{xy})}{1 - v_{xy}^2} \tag{12b}$$

$$\alpha_3 = \sqrt{\frac{\alpha_1 + \alpha_2}{2}}\left(\frac{1 - v_{xy}}{G_{xy}}\right) \tag{12c}$$

In Eqs. (12a)–(12c), the equivalent orthotropic properties can be determined from the stiffness or compliance matrix of a laminate (Tsai and Hahn, 1980).

Inserting Eq. (10) into Eq. (5) gives

$$\begin{aligned} &\frac{\mathrm{d}^2\alpha}{\mathrm{d}t^2} + \frac{1}{8\sqrt{m_p D^*}} \cdot \frac{3}{2} \cdot \beta k_h \cdot \alpha^{1/2} \cdot \frac{\mathrm{d}\alpha}{\mathrm{d}t} + \frac{k_h}{m_i} \cdot \alpha^{3/2} = 0 \\ &\alpha(0) = 0, \quad \dot{\alpha}(0) = V_0 \end{aligned} \tag{13}$$

Introducing the non-dimensional variables

$$\bar{\alpha} = \frac{\alpha}{V_0 T_e}, \qquad \bar{t} = \frac{t}{T_e} \tag{14}$$

where T_e is an unknown time constant needed to be determined for Hertzian contact law based on governing equation Eq. (13).

Then Eq. (13) becomes

$$\begin{aligned} &\frac{\mathrm{d}^2\bar{\alpha}}{\mathrm{d}\bar{t}^2} + \lambda_e \cdot \frac{3}{2} \cdot \bar{\alpha}^{1/2} \cdot \frac{\mathrm{d}\bar{\alpha}}{\mathrm{d}\bar{t}} + \bar{\alpha}^{3/2} = 0 \\ &\bar{\alpha}(0) = 0, \quad \dot{\bar{\alpha}}(0) = 1 \end{aligned} \tag{15}$$

where the coefficients

$$\lambda_e = \frac{(\beta k_h)^{2/5} \cdot V_0^{1/5} \cdot m_i^{3/5}}{8\sqrt{m_p}} \tag{16a}$$

$$T_e = \left(\frac{m_i}{\beta k_h \sqrt{V_0}}\right)^{2/5} \tag{16b}$$

Eq. (15) is a second-order nonlinear ordinary differential equation. The $\bar{\alpha}(\bar{t})$ can be solved numerically for different values of λ_e. The dimensionless indentation and contact force histories have been plotted for different values of λ_e, as shown in Figs. 2 and 3, respectively.

It can be seen that for an infinite plate with Hertzian contact law, the impact is governed by a single parameter λ_e that combines the effect of the contact stiffness, impact velocity, the mechanical and geometrical properties of the plate and the projectile. From Fig. 3, the highest contact force is obtained for $\lambda_e = 0$, where the plate is very rigid and the problem of the impact can be considered as impact on a half-space. As λ_e increases, the contact force history becomes more asymmetrical and the contract duration increases as the deformation of the plate becomes more significant.

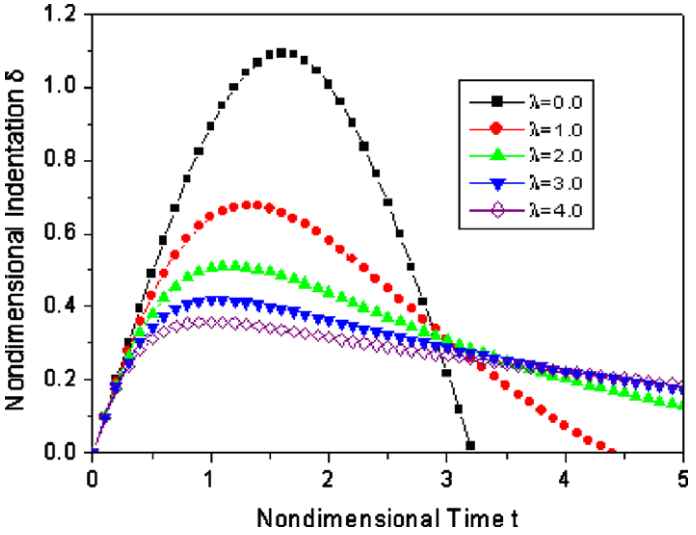

Fig. 2. Nondimensional indentation histories as a function of λ_e.

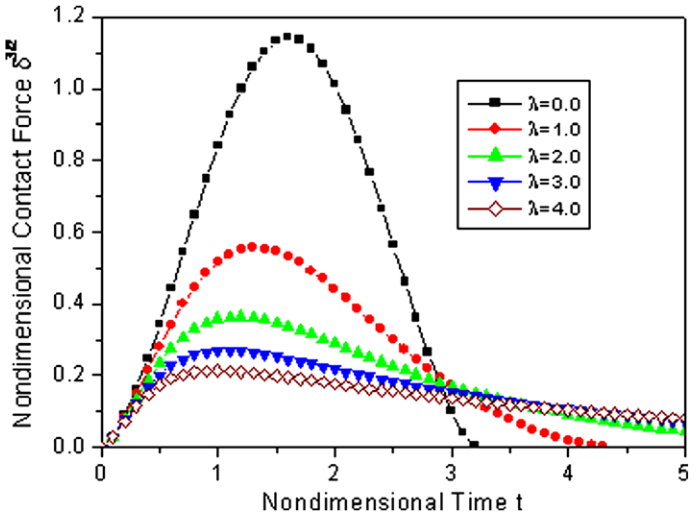

Fig. 3. Nondimensional contact force histories as a function of λ_e.

3.2. Elasto-plastic contact law

Hertzian-type contact laws were obtained from the elasto-static analysis of the contact between a sphere and an elastic half-space. Because permanent deformation is not taken into account in the formulation, they are only valid during the initial stages of the impact event. Therefore, a contact law incorporating damage effects is needed for an accurate modeling of contact force-deformation during impact.

In this study, the contact law accounting for permanent deformation proposed by Yigit and Christoforou (1994) is used. In this contact law, it is assumed the contact consists of three phases. The contact is assumed to be Hertzian for the first phase. For the second phase, the elastic–plastic behavior is assumed where the "yielding" point is exceeded. In case of fiber composites, "yielding" means a combination of different damage modes such as matrix crack and fiber tensile failure or buckling. Assuming that the deformations in the plane surface outside the contact region can be neglected, the slope of load-indentation curve after the critical indentation can be shown approximately as a constant, i.e., a nearly linear relationship between force and indentation exists (Abrate, 1998; Cairns, 1991). The third phase is assumed to be elastic Hertzian behavior again.

The quasi-static contact law for the three phases is given as following.

Phase I: Elastic loading

$$F(\alpha) = K_h \alpha^{3/2} \quad 0 \leqslant \alpha \leqslant \alpha_{cr} \tag{17}$$

Phase II: Elasto-plastic loading

$$F(\alpha) = K_y(\alpha - \alpha_{cr}) + K_h \alpha_{cr}^{3/2} \quad \alpha_{cr} \leqslant \alpha \leqslant \alpha_m \tag{18}$$

Phase III: Elastic unloading and reloading

$$F(\alpha) = K_h(\alpha^{3/2} - \alpha_m^{3/2} + \alpha_{cr}^{3/2}) + K_y(\alpha_m - \alpha_{cr}) \tag{19}$$

where α_{cr} is the critical indentation when material yields, and α_m is the maximum indentation when the unloading or restitution begins. α_{cr} was obtained from the contact stress distribution based on maximum fiber shear failure criterion (Poe and Illg, 1989; Yigit and Christoforou, 1994)

$$\alpha_{cr} = \frac{0.68 \cdot (2S_u)^2 \pi^2 R}{Q_\alpha^2} \tag{20}$$

where S_u is the interlaminar shear strength of laminated composites.

The slope of the elastic indentation curve at $\alpha = \alpha_{cr}$ is given by

$$K_y = 1.5 K_h \sqrt{\alpha_{cr}} \tag{21}$$

Substituting Eqs. (17)–(19) into Eq. (5), the governing equation of the indentation considering permanent indentation and damage effects can be obtained. For the elastic loading phase

$$\begin{aligned} &\frac{\mathrm{d}^2\alpha}{\mathrm{d}t^2} + \frac{1}{8\sqrt{m_p D^*}} \cdot \frac{3}{2} \cdot k_h \cdot \alpha^{1/2} \cdot \frac{\mathrm{d}\alpha}{\mathrm{d}t} + \frac{k_h}{m_i} \cdot \alpha^{3/2} = 0 \\ &\alpha(0) = 0, \quad \dot{\alpha}(0) = V_0, \quad 0 \leqslant \alpha \leqslant \alpha_{cr} \end{aligned} \tag{22}$$

For the elasto-plastic loading phase

$$\begin{aligned} &\frac{\mathrm{d}^2\alpha}{\mathrm{d}t^2} + \frac{1}{8\sqrt{m_p D^*}} \cdot K_y \cdot \frac{\mathrm{d}\alpha}{\mathrm{d}t} + \frac{K_y}{m_i} \cdot (\alpha - \alpha_{cr}) + \frac{K_h}{m_i} \cdot \alpha_{cr}^{3/2} = 0 \\ &\alpha(t_{cr}) = \alpha_{cr}, \quad \dot{\alpha}(t_{cr}) = V_{cr}, \quad \dot{\alpha}(t_m) = 0, \quad \alpha_{cr} \leqslant \alpha \leqslant \alpha_m \end{aligned} \tag{23}$$

For the elastic unloading phase

$$\begin{aligned} &\frac{\mathrm{d}^2\alpha}{\mathrm{d}t^2} + \frac{1}{8\sqrt{m_p D^*}} \cdot K_h \cdot \frac{3}{2} \cdot \alpha^{1/2} \cdot \frac{\mathrm{d}\alpha}{\mathrm{d}t} + \frac{K_h}{m_i} \cdot \left(\alpha^{3/2} - \alpha_m^{3/2} + \alpha_{cr}^{3/2}\right) + \frac{K_y}{m_i} \cdot (\alpha_m - \alpha_{cr}) = 0 \\ &\alpha(t_m) = \alpha_m, \quad \dot{\alpha}(t_m) = 0, \quad \alpha_f \leqslant \alpha \leqslant \alpha_m \end{aligned} \tag{24}$$

In Eqs. (23) and (24), t_{cr} and t_m are the time to reach critical indentation and maximum indentation, respectively. α_{cr}, α_m and α_f are the critical indentation, maximum indentation and permanent indentation, respectively and

$$\alpha_f = \alpha_m - \alpha_{cr} \tag{25}$$

3.3. Linearized elasto-plastic contact law

As shown in Eq. (13) and Eqs. (22)–(24), due to the nonlinearity of the elastic and elasto-plastic contact law, an analytical solution is generally not possible. One method of contact stiffness linearization is to obtain an equivalent linear stiffness for a single degree-of-freedom lumped model which will result in the same maximum contact force (Bucinell et al., 1991). Since the linearized contact stiffness only depends on the maximum contact force, it may not be adequate for situations where the details of the contact law and permanent deformations are important.

Another method for the situation where permanent deformation is present is to linearize each phase of the contact law separately with very good results (Yigit and Christoforou, 1995). However, for most composite materials, damage occurs early in the loading phase and most of the local response is dominated by the second phase of the contact law (Yigit and Christoforou, 1994). Therefore, it is worthwhile to consider only the linearization of the elasto-plastic phase which is already linear. The linearized contact law can be written as

$$F(\alpha) = K_y \alpha \tag{26}$$

Substituting the linearized contact law into the governing equation for indentation Eq. (5), the governing equation becomes

$$\begin{aligned} &\frac{\mathrm{d}^2\alpha}{\mathrm{d}t^2} + \frac{1}{8\sqrt{m_p D^*}} \cdot K_y \cdot \frac{\mathrm{d}\alpha}{\mathrm{d}t} + \frac{K_y}{m_i} \cdot \alpha = 0 \\ &\alpha(0) = 0, \quad \dot{\alpha}(0) = V_0 \end{aligned} \tag{27}$$

Introducing nondimensional variables similar to Eq. (14)

$$\bar{\alpha} = \frac{\alpha}{V_0 T_p}, \qquad \bar{t} = \frac{t}{T_p} \tag{28}$$

where T_p is an unknown time constant needed to be determined for Elasto-plastic contact law based on governing equation Eq. (27).

Then Eq. (27) can be written as

$$\begin{aligned} &\frac{\mathrm{d}^2\bar{\alpha}}{\mathrm{d}\bar{t}^2} + \lambda_p \cdot \frac{\mathrm{d}\bar{\alpha}}{\mathrm{d}\bar{t}} + \bar{\alpha} = 0 \\ &\bar{\alpha}(0) = 0, \quad \dot{\bar{\alpha}}(0) = 1 \end{aligned} \tag{29}$$

with the coefficients

$$\lambda_p = \frac{1}{8}\sqrt{\frac{K_y m_i}{m_p D^*}} \text{ and } T_p = \sqrt{\frac{m_i}{K_y}} \tag{30}$$

Eq. (29) is the equation of motion for single degree of freedom system with viscous damping (Abrate, 1998). By introducing the variable $\eta = \lambda_p/2$ and distinguishing different range of values of η, the closed-form solution of Eq. (29) can be obtained

$$\text{Under-damping}: \ \eta < 1 \quad \bar{\alpha} = \mathrm{e}^{-\eta\bar{t}} \sin(\sqrt{1-\eta^2} \cdot \bar{t}) / \sqrt{1-\eta^2} \tag{31a}$$

$$\text{Critical-damping}: \ \eta = 1 \quad \bar{\alpha} = \bar{t}\mathrm{e}^{-\bar{t}} \tag{31b}$$

$$\text{Over-damping}: \ \eta > 1 \quad \bar{\alpha} = \mathrm{e}^{-\eta\bar{t}} \sinh(\sqrt{\eta^2-1} \cdot \bar{t}) / \sqrt{\eta^2-1} \tag{31c}$$

The physical indentation time history can be obtained by multiplying dimensionless quantity with the physical constants in Eq. (28)

$$\alpha(t) = V_0 \cdot T_p \cdot \bar{\alpha}(t/T_p) \tag{32}$$

From Eqs. (26) and (32), the physical contact force time history is given by

$$\eta < 1: \quad F(t) = K_y V_0 T_p \cdot \mathrm{e}^{-\eta \cdot t/T_p} \cdot \sin\left(\sqrt{1-\eta^2} \cdot t/T_p\right)/\sqrt{1-\eta^2} \tag{33a}$$

$$\eta = 1: \quad F(t) = K_y V_0 t \cdot \mathrm{e}^{-t/T_p} \tag{33b}$$

$$\eta > 1: \quad F(t) = K_y V_0 T_p \cdot \mathrm{e}^{-\eta t/T_p} \sinh\left(\sqrt{\eta^2-1} \cdot t/T_p\right)/\sqrt{\eta^2-1} \tag{33c}$$

From Eq. (1), the physical central displacement of the plate can be written as

$$w_p(0,0,t) = \frac{m_i V_0}{8\sqrt{m_p D^*}} \int_0^{\bar{t}} \bar{\alpha}(\bar{t}) \mathrm{d}\bar{\tau} \tag{34}$$

Combining Eqs. (31a)–(31c) with Eq. (34), the central displacement of the plate for under-damping case can be obtained as

$$w_p(0,0,t) = \frac{m_i V_0}{8\sqrt{m_p D^*}} \cdot \left[1 - \mathrm{e}^{-\eta t/T_p} \cdot \left(\cos(\sqrt{1-\eta^2} \cdot t/T_p) + \frac{\eta \sin(\sqrt{1-\eta^2} \cdot t/T_p)}{\sqrt{1-\eta^2}}\right)\right] \tag{35a}$$

The center displacement of the plate for critical-damping case is

$$w_p(0,0,t) = \frac{m_i V_0}{8\sqrt{m_p D^*}} \cdot \left[1 - \mathrm{e}^{-t/Tp} \cdot (1 + t/T_p)\right] \tag{35b}$$

The center displacement of the plate for over-damping case is

$$w_p(0,0,t) = \frac{m_i V_0}{8\sqrt{m_p D^*}} \cdot \left[1 - \mathrm{e}^{-\eta t/T_p} \cdot \left(\cosh(\sqrt{\eta^2-1} \cdot t/T_p) + \frac{\eta \sinh(\sqrt{\eta^2-1} \cdot t/T_p)}{\sqrt{\eta^2-1}}\right)\right] \tag{35c}$$

4. Delamination onset prediction

Experimental and numerical results indicate that the threshold force can be used at least as a qualitative indicator of delamination onset under small mass impacts (Beks, 1996). In this study, based on the closed form solution of the contact force time history, the peak contact force is obtained from the characteristics of the contact force history curve. Fig. 4 shows the non-dimensional indentation as a function of non-dimensional time for under-damping, critical damping and over-damping three cases. It can be seen that the peak value of contact force can be obtained as

$$F_{\mathrm{peak}} = K_y \alpha_{\max} = K_y \alpha(t)|_{\frac{\mathrm{d}\alpha}{\mathrm{d}t}=0} \tag{36}$$

After some algebraic manipulations, the peak contact force can be obtained for three different cases

$$\eta < 1: \quad F_{\mathrm{peak}} = K_y \cdot V_0 \cdot T_p \cdot \mathrm{e}^{-\frac{\eta \ \mathrm{Arc}\cos(\eta)}{\sqrt{1-\eta^2}}} \tag{37a}$$

$$\eta = 1: \quad F_{\mathrm{peak}} = K_y \cdot V_0 \cdot T_p \cdot \frac{1}{e} \tag{37b}$$

$$\eta > 1: \quad F_{\mathrm{peak}} = K_y \cdot V_0 \cdot T_p \cdot \frac{(-1+\eta\xi) \cdot (-1+2\eta\xi)^{\frac{1}{-2+2\eta\psi}}}{\sqrt{\eta^2-1}} \tag{37c}$$

where $\xi = \eta + \sqrt{\eta^2-1}$ and $\psi = \eta - \sqrt{\eta^2-1}$.

Davies and Robinson (1992) proposed an approach to deal with the prediction of the threshold value of the contact force that corresponds to damage initiation. It was shown that when the damage area is plotted versus

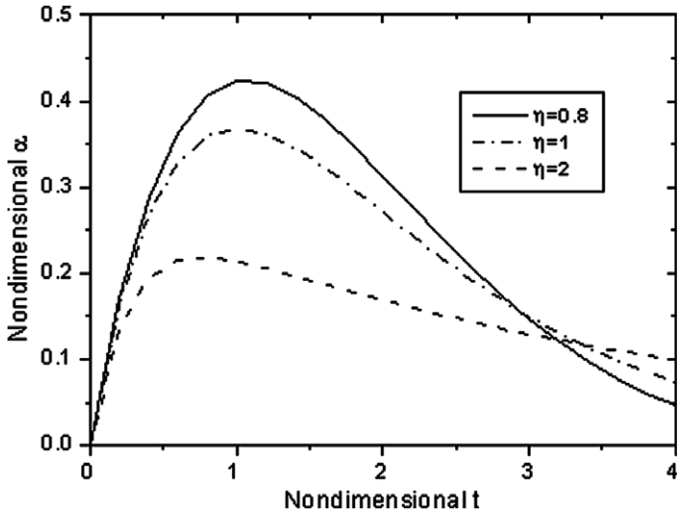

Fig. 4. Non-dimensional indentation vs. Time for three cases.

the maximum impact force, there is a clear sudden increase in damage size once the load reaches a critical value. This method has been used successfully to predict the onset of delamination damage for several quasi-isotropic graphite-epoxy laminates. The simple model for estimating this critical load is shown in Fig. 5. It can be seen that at the threshold value of impact force, there is an unstable crack propagation leading to large delamination size. This will cause the impact force drop suddenly in the response representing the loss of transverse stiffness. After this, the delamination size increases linearly with the force indicating stable delamination growth. For quasi-static axisymmetric delamination growth in a centrally loaded clamped plate, the threshold load for delamination can be derived from this model as (Davies et al., 1994).

$$F_{\mathrm{del}}^{\mathrm{stat}} = \pi\sqrt{32D^{*}G_{IIc}/3} \tag{38}$$

where G_{IIc} is the critical energy release rate for mode II fracture. The independence of delamination size and boundary conditions implies that the delamination threshold load is applicable to impact situations where inertial effects may be neglected (Olsson, 2003). The delamination threshold load considering inertial effects was given as (Olsson et al., 2006):

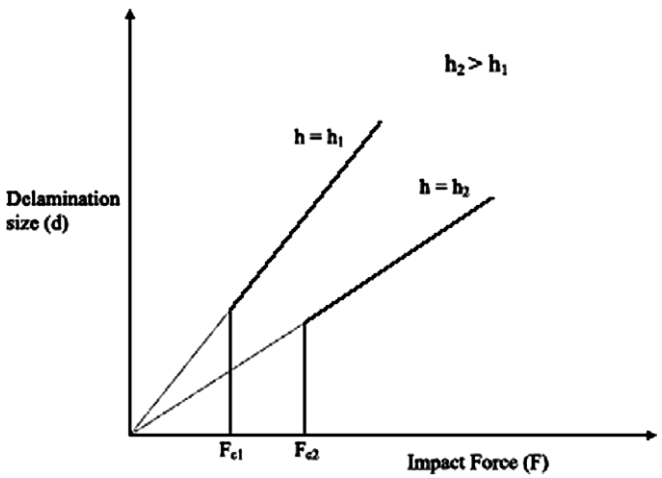

Fig. 5. Damage size as a function of impact force for plates (Christoforou, 2001).

$$F_{\mathrm{del}}^{\mathrm{dyn}} = F_{\mathrm{del}}^{\mathrm{stat}} \Big/ \sqrt{1 - 7\pi^2/216} \approx 1.213 F_{\mathrm{del}}^{\mathrm{stat}} \tag{39}$$

Combining Eqs. (37) to (39), the threshold velocity for a given plate and projectile can be predicted with closed-form solution as following

$$\eta < 1: \quad V_{\mathrm{th}} = F_{\mathrm{del}}^{\mathrm{dyn}} \Big/ \left(K_y \cdot T_p \cdot \mathrm{e}^{-\frac{\eta\ \mathrm{Arc}\cos(\eta)}{\sqrt{1-\eta^2}}} \right). \tag{40a}$$

$$\eta = 1: \quad V_{\mathrm{th}} = F_{\mathrm{del}}^{\mathrm{dyn}} \Big/ \left(K_y \cdot T_p \cdot \frac{1}{e} \right) \tag{40b}$$

$$\eta > 1: \quad V_{\mathrm{th}} = F_{\mathrm{del}}^{\mathrm{dyn}} \Big/ \left(K_y \cdot T_p \cdot \frac{(-1+\eta\xi)\cdot(-1+2\eta\xi)^{\frac{1}{-2+2\eta\psi}}}{\sqrt{\eta^2-1}} \right) \tag{40c}$$

5. Application examples: influence of contact laws

A symmetric cross-ply $[0/90/0/90/0]_s$ T300/934 graphite/epoxy composite plate is analyzed to illustrate the effect of different contact laws on the impact responses. The material properties, geometry and impact conditions for the impact problem are given in Table 1 (Cairns and Lagace, 1989). For the first case, the initial velocity of the projectile is 3.0 m/s. The calculated impact parameter for elastic and elasto-plastic contact law is $\lambda_e = 2.07$ and $\lambda_p = 1.71$, respectively. The comparison of the impact force history, contact law and plate deformation using different contact laws is shown in Figs. 6–8, respectively. In Figs. 6–8, the elastic curves and

Table 1
Geometrical and material properties of the composite plate

Plate: $[0/90/0/90/0]_s$ T300/934 graphite/epoxy composite plate, simple supported
Plate size: 200 mm × 200 mm
$D_{11} = 154.9$ Nm, $D_{12} = 4.760$ Nm, $m_{\mathrm{p}} = 4.132$ kg/m^2, $D_{22} = 91.4$ Nm
$D_{66} = 8.970$ Nm
Projectile 1: $R = 6.35$ mm, $V_0 = 3.0$ m/s, $m_{\mathrm{i}} = 8.30$ g
Projectile 2: $R = 6.35$ mm, $V_0 = 30$ m/s, $m_{\mathrm{i}} = 8.30$ g
Impact Parameter: $K_{\mathrm{h}} = 1.033\mathrm{E}9$ N/m$^{3/2}$, $\lambda_{e1} = 2.07$, $\lambda_{e2} = 3.30$, $\lambda_p = 1.71$

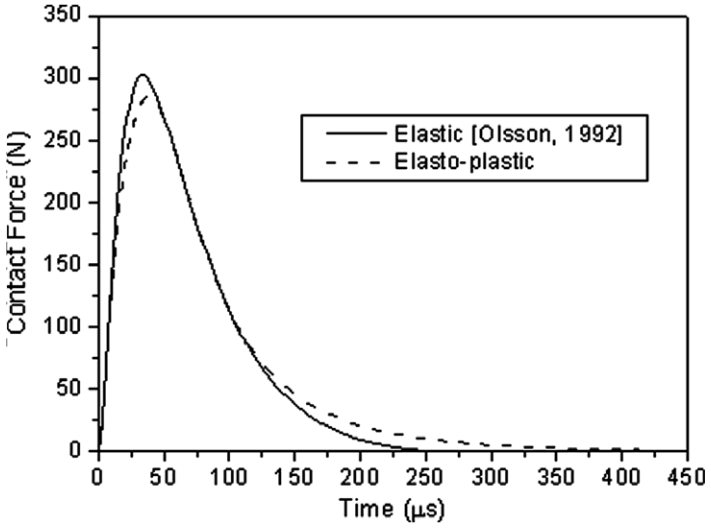

Fig. 6. Comparison of contact force history ($\lambda_e = 2.07$).

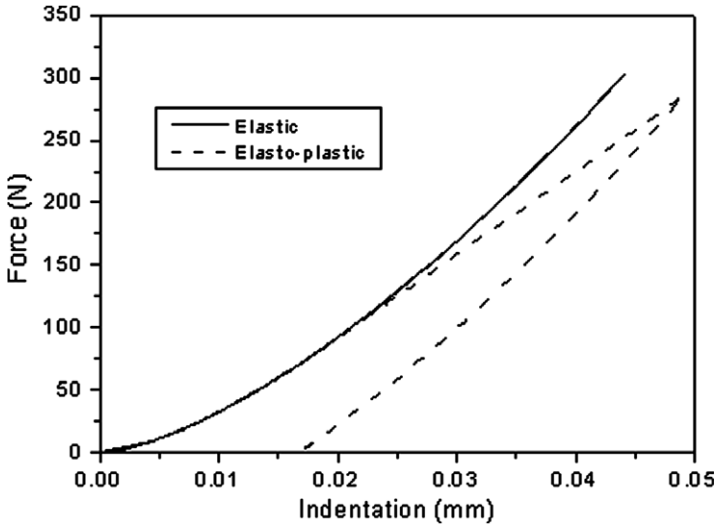

Fig. 7. Comparison of contact law ($\lambda_e = 2.07$).

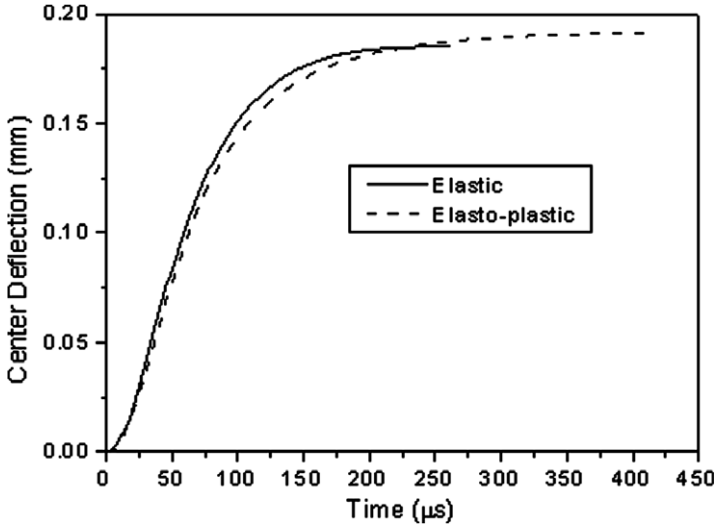

Fig. 8. Comparison of center deflection of plate ($\lambda_e = 2.07$).

the elasto-plastic curves are based on the solutions of the equations of motion in Eq. (13) and Eqs. (22)–(24), respectively. It demonstrates that elasto-plastic contact reduces the contact force and increases the contact duration. There is significant amount of permanent deformation due to local impact damage during elasto-plastic impact, which is more consistent with existing experimental data (Swanson and Rezaee, 1990).

In the second case, the initial velocity of the projectile is increased to 30 m/s by keeping all other parameters the same as before. The calculated impact parameter for elastic and elasto-plastic contact law is $\lambda_e = 3.30$ and $\lambda_p = 1.71$, respectively. The comparison of impact force history, contact law and plate deflection from elastic and elasto-plastic impact is shown in Figs. 9–11, respectively. In Figs. 9–11, the elastic curves and the elasto-plastic curves are based on the solutions of the equations of motion in Eq. (13) and Eqs. (22)–(24), respectively. It can be seen that the use of elasto-plastic contact law can significantly change the contact force history and plate center deflection when the velocity of projectile reaches medium velocity. The peak plate central displacements associated with permanent indentations are significantly less compared to the elastic contact

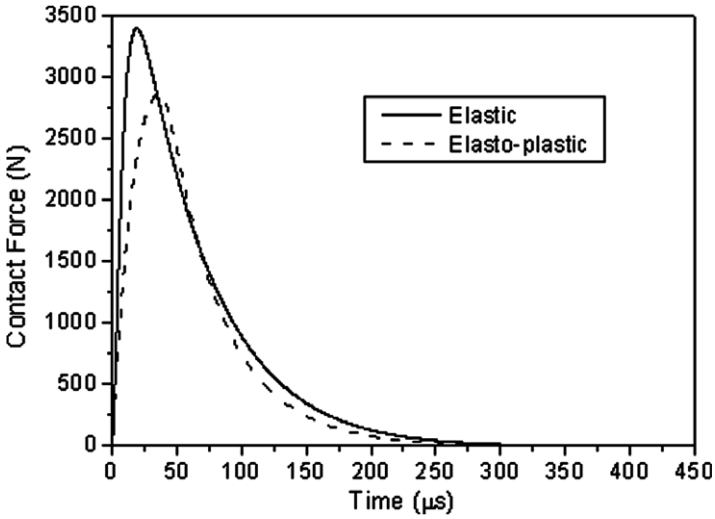

Fig. 9. Comparison of contact force history ($\lambda_e = 3.30$).

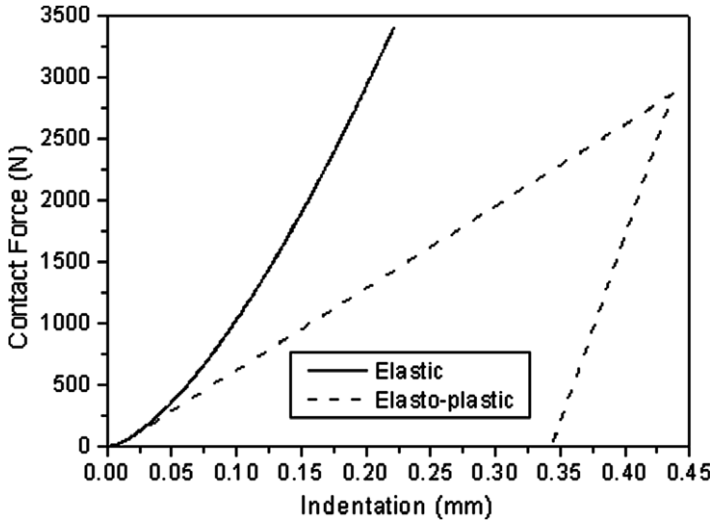

Fig. 10. Comparison of contact law ($\lambda_e = 3.3$).

solutions because of the smaller contact force resulting at the contact region. Similar conclusions were obtained for elastic isotropic plates by Chattopadhyay and Saxena (1991).

6. Application examples: Delamination threshold

The closed-form prediction of the contact force history for the first case in Section 5 is demonstrated in Fig. 12, where the elasto-plastic and closed-form curves are based on the solutions equations of motion in Eqs. (22)–(24) and Eq. (33), respectively. It is clearly shown that the linearized elasto-plastic contact law can predict the peak contact force quite well. The predicted peak contact force can then be combined with the delamination threshold load considering dynamic inertia effect, Eq. (39), to predict the delamination threshold velocity for small mass impacts. Several experimental studies on symmetric composite laminated plates impacted by small mass steel or aluminum impactor were compared with the closed-form predictions from current methodology. Table 2 shows a list of the assumed material properties for the laminates and impactors (Olsson, 2003).

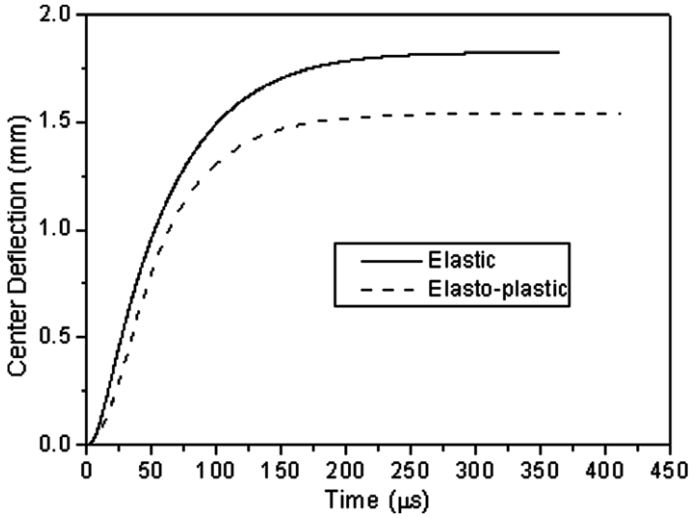

Fig. 11. Comparison of center deflection ($\lambda_e = 3.3$).

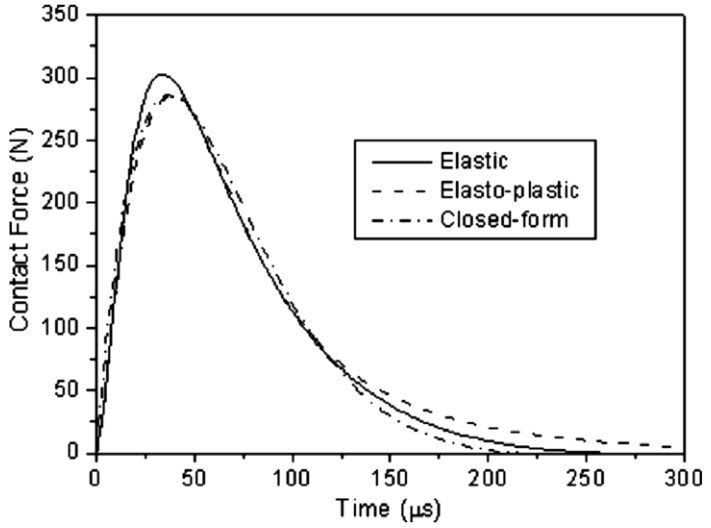

Fig. 12. Comparison of contact force history ($\lambda_e = 2.07$, $\lambda_p = 1.71$).

Table 2
Material properties for experimental validation

Material	E_{11} (GPa)	E_{22} (GPa)	G_{12} (GPa)	G_{23} (GPa)	ν_{12}	ν_{23}	ρ (kg/m^3)	t_{ply} (mm)	G_{IIc} (J/m^2)
Aluminum	71	71	27	27	0.30	0.30	2790	–	–
Steel	206	206	79	79	0.30	0.30	7850	–	–
HTA/6376C	137	10.4	5.2	3.5	0.30	0.51	1620	0.130	400
T300/5208	132	10.8	5.6	4.4	0.24	0.50	1600	0.127	300
AS4/2220-3	123	11.1	6.3	3.7	0.29	0.50	1600	0.129	510
XAS/914C	145	9.5	5.6	3.6	0.31	0.50	1600	0.125	416
AS4/PEEK	137	10.6	5.4	3.5	0.40	0.50	1600	0.135	1959

Interlaminar shear strength is defined as the shear stress at rupture, where the plane of fracture is located between the layer interfaces of a composite laminate. (Pahr et al., 2002) reviewed a number of test methods for the measurement of interlaminar shear strength. It was shown that the experimental interlaminar shear

Table 3
Shear strength of the laminate (S_u)

	AS4/PEEK	AS4/2220-3	T300/5208	HTA/6376C	XAS/914C
Fiber Volume Ratio	0.58	0.63	0.65	0.60	0.60
S_u (MPa)	157	110	101	93	95

Table 4
Measured and Predicted Delamination Threshold Velocities

Plate	Layup	h (mm)	G_{IIc} (J/m^2)	Q_{zp} (GPa)	m_p (Kg/m^2)	m_i (g)	$V_{\exp}$ (m/s)	V^a_{pred} (m/s)	V^b_{pred} (m/s)
HTA /6376C	$[(0/\pm45/90)_s/(90/\mp45/0)_s]_3$	6.24	400	11.36	9.85	10.2	28 (Olsson, 2003)	32	34.2
AS4 /PEEK	$[0_3/45_3/90_3/-45_3]_s$	3.24	1959	11.47	5.18	1.9	46 (Morita et al., 1997)	68	73.2
T300 /5208	$(0/\pm45/90)_{6s}$	6.2	300	12.74	9.75	3.0	38 (Williams, 1984)	38	57
AS4 /2220-3	$(0/\pm45/90)_{6s}$	6.2	510	12.06	9.91	3.0	55 (Williams, 1984)	46	71.2
XAS /914C	$[0_2/\pm45]_{2s}$	2.0	416	11.05	3.2	0.9	30 (Cantwell and Morton, 1989)	34	39.4
XAS /914C	$[0/90]_{2s}$	1.0	416	11.05	1.6	0.9	33 (Cantwell, 1988)	32	32.4

V^a_{pred}: prediction from reference (Olsson et al., 2006); V^b_{pred}: prediction from present study.

strength values represent a lower bound for the true interlaminar shear strength. The interlaminar shear strength values for the laminates used in this study, as shown in Table 3, are obtained from manufacture's data and available experimental data (Choi and Chang, 1992; Christoforou and Yigit, 1998).

Table 4 illustrates the comparison between predicted and measured delamination threshold velocities in a number of experimental studies. In all of the calculations, the effects of plate finite thickness and effective modulus based on transversely isotropic material properties were included. Since the ratio of plate thickness to contact radius is significantly larger than 2.0 for all the investigated laminated plates, the empirical constant β was assumed as 1.0 for all cases (Swanson, 2005). Dynamic inertia effect of the impacts was also included in the current predictions. Very good agreement with experimental observations is obtained. The predictions from current theory are also compared well with the predictions from asymptotic solutions by Olsson et al. (2006). The present approach for prediction of delamination onset is based on elasto-plastic contact law including the effect of damage and permanent indentation, which was not considered by existing literatures in the prediction of delamination.

7. Conclusions

In this paper, a linearized elasto-plastic contact law including permanent indentation and damage effects was used to obtain the closed-form approximations of the small mass impact response of composite laminate. It was shown that the use of elasto-plastic contact law can significantly change the impact response when the velocity of projectile reaches medium velocity. Based on the peak contact forces from the linearized elasto-plastic contact law as well as a quasi-static delamination threshold load criterion, the delamination threshold velocity was obtained analytically. It is demonstrated that the predictions for delamination threshold velocity are in good agreement with experimental values for a wide range of test cases and existing literatures. Further experiments and analysis are required to fully verify the validity and limitations of the methodology. The analytical peak contact force and delamination threshold velocity would be useful for designers who prefer closed form solutions for the criticality of small mass impacts.

Acknowledgements

The support of NASA Gleen Research Center and The University of Akron for this study is greatly acknowledged.

References

Abrate, S., 1991. Impact on laminated composite materials. Applied Mechanics Reviews 44 (4), 155–189.
Abrate, S., 1998. Impact on Composite Structures. Cambridge University Press.
Beks, F-A., 1996. Examination of impact response and damage of composite laminates. FFATN 1996-29, Bromma: The Aeronautical Research Institute of Sweden.
Bucinell, R.B., Nuismer, R.J., Koury, J.L., 1991. Response of composites plates to quasi-static impact events. In: Composite Materials: Fatigue and Fracture (vol. 3), ASTM STP 1110, ASTM, Philadelphia, PA, pp. 528–549.
Cairns, D.S., 1991. A Simple, elasto-plastic contact law for composites. Journal of Reinforced Plastics and Composites 10 (4), 423–433.
Cairns, D.S., Lagace, P.A., 1989. Transient response of graphite/epoxy and kevlar/epoxy laminates subjected to impact. AIAA Journal 27 (11), 1590–1596.
Cantwell, W.J., 1988. The influence of target geometry on the high velocity impact response of CFRP. Composite Structures 10 (3), 247–265.
Cantwell, W.J., Morton, J., 1989. Comparison of the low and high velocity impact response of CFRP. Composites 20 (6), 545–551.
Chattopadhyay, S., Saxena, R., 1991. Combined effects of shear deformation and permanent indentation on the impact response of elastic plates. International Journal of Solids and Structures 27 (13), 1739–1745.
Choi, H.Y., Chang, F.K., 1992. A Model for predicting damage in graphite/epoxy laminated composites resulting from low-velocity point impact. Journal of Composite Materials 26 (14), 2134–2169.
Christoforou, A.P., 2001. Impact dynamics and damage in composite structures. Composite Structures 52 (2), 181–188.
Christoforou, A.P., Yigit, A.S., 1998. Characterization of impact in composite plates. Composite Structures 43 (1), 15–24.
Christopherson, J., Mahinfalah, M., Jazar, G.N., Aagaah, M.R., 2005. An investigation on the effect of small mass impact on sandwich composite plates. Composite Structures 67 (3), 299–306.
Davies, G.A.O., Robinson, P., 1992. Predicting failure by debonding/delamination. In: Debonding/Delamination of Composites, AGARD-CP-530, 5-1-28.
Davies, G.A.O., Zhang, X., Zhou, G., Watson, S., 1994. Numerical modeling of impact damage. Composites 25 (5), 342–350.
Goldsmith, G., 1960. Impact: The Theory and Physical Behavior of Colliding Solids. Edward Arnold, London.
Mittal, R.K., 1987. Effect of transverse shear on the behavior of a beam under dynamic loading. Z. Angew. Math. Mech. Journal of Applied Mathematics and Mechanics 67 (3), 175–181.
Morita, H., Adachi, T., Tateishi, Y., Matsumoto, H., 1997. Characterization of impact damage resistance of CF/PEEK and CF/toughened epoxy laminates under low and high velocity impact tests. Journal of Reinforced Plastic and Composites 16 (2), 131–143.
Olsson, R., 1992. Impact response of orthotropic composite plates predicted from a one-parameter differential equation. AIAA Journal 30 (6), 1587–1596.
Olsson, R., 2000. Mass criterion for wave controlled impact response of composite plates. Composites Part A: Applied Science and Manufacturing 31 (8), 879–887, Corrigendum in Composites Part A: Applied Science and Manufacturing 32 (2), 291.
Olsson, R., 2001. Analytical prediction of large mass impact damage in composite laminates. Composites Part A: Applied Science and Manufacturing 32 (9), 1207–1215.
Olsson, R., 2003. Closed form prediction of peak load and delamination onset under small mass impact. Composite Structures 59 (3), 341–349.
Olsson, R., Donadon, M.V., Falzon, B.G., 2006. Delamination threshold load for dynamic impact on plates. International Journal of Solids and Structures 43 (10), 3124–3141.
Pahr, D.H., Rammerstorfer, F.G., Rosenkranz, P., Humer, K., Weber, H.W., 2002. A study of short-beam-shear and double-lap-shear specimens of glass fabric/epoxy composites. Composites Part B: Engineering 33 (2), 125–132.
Poe, C.C., Jr., Illg, W., 1989. Strength of a thick graphite/epoxy rocket motor case after impact by a blunt object. In:Test Methods for Design Allowables for Fibrous Composites: vol. 2, ASTM STP 1003, ASTM, Philadelphia, pp. 150–179.
Suemasu, H., Kerth, S., Maier, M., 1994. Indentation of spherical head indentors on transversely isotropic composite plates. Journal of Composite Materials 28 (17), 1723–1739.
Swanson, S.R., 2005. Contact deformation and stress in orthotropic plates. Composites Part A: Applied Science and Manufacturing 36 (10), 1421–1429.
Swanson, S.R., Rezaee, H.G., 1990. Strength loss in composites from lateral contact loads. Composites Science and Technology 38 (1), 43–54.
Tan, T.M., Sun, C.T., 1985. Use of statical indentation laws in the impact analysis of laminated composite plates. Journal of Applied Mechanics 52 (1), 6–12.
Tsai, S.W., Hahn, H.T., 1980. Introduction to Composite Materials. Technomic Publishing Company, Inc.
Turner, J.R., 1979. Contact on a transversely isotropic half-space, or between two transversely isotropic bodies. International Journal of Solids and Structures 16, 409–419.

Williams, J.G., 1984. Effect of impact damage and open holes on the compression strength of tough resin/high strain fiber laminates, Tough Composite Materials, NASA CP 2334, pp. 61–79.

Yang, S.H., Sun, C.T., 1982. Indentation law for composite laminates. Composite Materials: Testing and Design (6th Conference, Editor: M. Daniel). ASTM STP 787, ASTM, Philadelphia, PA, pp. 425–449.

Yigit, A.S., Christoforou, A.P., 1994. On the impact of a spherical indenter and an elastic–plastic transversely isotropic half-space. Composites Engineering 4 (11), 1143–1152.

Yigit, A.S., Christoforou, A.P., 1995. On the impact between a rigid sphere and a thin composite laminate supported by a rigid substrate. Composite Structures 30 (2), 169–177.